Libyan Journal of Science & Technology 11:2 (2020) 110–119

Faculty of Science - University of Benghazi

Libyan Journal of Science & Technology

journal home page: www.sc.uob.edu.ly/pages/page/77

Oxidative dehydrogenation of Propane over vanadium catalysts

Hanan M. Eghreibeel[a], Issa M. Korbag*[,a], Halima, F. Alamary[b], Sabri S. Mahmoud[c], Ayman Y. Hammoudeh[c]

[a]*Department of Chemistry, Faculty of Arts and Sciences, University of Benghazi, Al Kufrah, Libya*

[b]*Department of Chemistry, Faculty of Arts and Sciences, University of Benghazi, Benghazi, Libya*

[c]*Department of Chemistry, Faculty of Science, University of Yarmouk, Irbid, Jordan*

Highlights

- **Vanadium catalysts were very active in the oxidation of propane and very selective to propene.**
- **All vanadium catalysts containing Mg in their composition were active in the oxidation of propane and selective to propene (oxidative dehydrogenation).**
- **All catalysts that contain on orthovanadate phase in composition were active in convert propane to propene (oxidative dehydrogenation).**
- **The catalyst of VO_x/ γ- Al_2O_3 was the most selective towards propene (84%), while V_2O_5-Ni-O/γ- Al_2O_3 catalyst was the most active catalyst in the oxidation of propane (98% conv).**

ARTICLE INFO

Article history:

Received 02 March 2020
Revised 12 July 2020
Accepted 08 October 2020

Keywords:

Oxidative Dehydrogenation; Vanadium Catalysts, XRD, IR, TEM

**Address of correspondence:*

E-mail address: issa.omar@uob.edu.ly

I. M. Korbag

ABSTRACT

A series of vanadium catalysts used for the propane oxidative dehydrogenation was synthesized by the adsorption equilibrium method and impregnation method. Several techniques such as XRD, IR spectroscopy, and TEM were applied to characterize physicochemical properties. The XRD diffraction patterns of the *V-Mg-O*, *V-Ni-O*, *V-Ni-Mg-O* and V_2O_5-Ni-O/γ-Al_2O_3 catalysts show the presence of orthovanadate phase. IR characterizations results of V-Mg-O and V-Ni-O agree with those of XRD, indicating the presence of the orthovanadate phase. TEM study shows that the particle size of V-Ni-Mg-O is around 46-192 nm, while V_2O_5-Ni-O/ γ- Al_2O_3 and V-Ni-O catalysts is around 14-196 nm. The structures of the reaction products were confirmed by ^{1}H-NMR which shows clearly the presence propene (oxidative dehydrogenation) in all catalysts, but by different ratios, such V_2O_5-Ni-Mg-O/γ-Al_2O_3 catalyst was the best catalyst in propene production at lower temperature 500°C. In additional, ethylene production through using V-Mg-O, V-Ni-O, V-Ni-Mg-O, V_2O_5-Ni-Mg-O/γ- Al_2O_3 and V_2O_5-Mg-O/γ-Al_2O_3 catalysts, and methane that indicates an occurrence (hydrogenolysis of propane) through the reaction for all catalysts, exception V_2O_5-Ni-O/ γ- Al_2O_3 and VO_x /γ-Al_2O_3 catalysts. The activity and selectivity of vanadium catalysts for propene production were also discussed in detail.

1. Introduction

The oxidation of alkanes is of great importance because of the economic benefits of using paraffin for the production of important base chemicals (Haracleous *et al.,* 2005). Propane selective oxidative dehydrogenation to propene by using different catalysts (Mishakov *et al*., 2009) and/or selective oxidation to acrolein or acrylic acid has been extensively studied in the last 20 years in industry (Dimitratos and Vedrine, 2003). The increasing demand for propylene, an important intermediate used extensively in the petrochemical industry, has led to finding an alternative to the conventional dehydrogenation process (Barsan and Thyrion, 2003). The propylene yields are not sufficiently high to satisfy the demands of the industrial catalytic processes due to propylene cracking into ethylene and methane (Pavlova *et al*., 2003). So that the oxidation of propane applied technique to destroy volatile organic compounds (pollutants) usually found in the atmosphere of all urban and industrial areas (Balcaen *et al*., 2011; Bouazza *et al*., 2008). Supported vanadium oxides are frequently used as catalysts in partial oxidation reactions. In these catalysts, Al_2O_3, TiO_2, SiO_2 and ZrO_2, are commonly used as supports (Routray *et al*., 2004). Supported vanadium oxides have been studied as catalysts for propane, n-butane, cyclohexane, and ethylbenzene oxidations. The activity and selectivity of these catalysts depend on the nature of support and on vanadium dispersion, vanadium concentration, and maybe also influenced by the treatment conditions (Mattos *et al*., 2002; Tapia *et al*., 2005). Nanostructured vanadium oxides have been extensively studied because they offer a greater potential for improving properties and find applications in many fields such as microelectronic, batteries, sensing devices, electrical conductors, magnetism … etc. So that a wide range of vanadium oxides have been obtained via the hydrothermal treatment of aqueous vanadium pentoxide solutions (Lu *et al*., 2004; Livage, 2010; Magon *et al*., 2012).

This study aims at investigating the catalytic performance of various vanadium mixed metal oxides and γ-Al_2O_3 supported vanadium oxides in the oxidation of propane (total oxidation), as well as, in the conversion of propane to propene (oxidative dehydrogenation), and correlating the catalytic behavior (activity and selectivity) of these oxides with their physicochemical characteristics. The effect of various parameters (catalyst composition, temperature, flow rates, partial pressures and pretreatment conditions) on the catalytic behavior of these oxides will be studied.

 ISSN 2663-1407; National Library of Libya, Legal number: 390/2018

2. Experimental Procedure

2.1. Materials

The materials used in this paper are Magnesium hydroxide (95%, Sigma Aldrich), Ammonium metavanadate anhydrates (99%, Sigma Aldrich), gamma-alumina (γ-Al_2O_3) (99.99%, Sigma Aldrich), Nickel (II) acetate hydrate (98%, Sigma Aldrich), aqueous ammonia (99.98%, Sigma Aldrich), and Aqua regia.

2.2. Catalyst preparation.

2.2.1. Preparation of V-Mg-O catalyst

1.5960 g of magnesium hydroxide powder was added to a basic hot aqueous solution containing 2.1335 g of ammonium metavanadate (NH_4VO_3) was dissolved in 120 ml distilled water in a 250 ml beaker. The pH was adjusted to pH=9 by adding aqueous ammonia. The mixture was stirred for one hour. The resulting suspension was evaporated to dryness at 85°C and then followed by further drying at 95°C for twelve hours. The dried powder was crushed and calcined under an oxygen atmosphere at 600°C for four hours (Mattos *et al.*, 2002).

2.2.2. Preparation of VO_X/ γ-Al_2O_3 Catalyst.

VO_X/ γ-Al_2O_3 catalyst was prepared by the adsorption equilibrium method. 6.00 g of γ-Al_2O_3 calcined under O_2 atmosphere at 500°C for one hour, and then added to 200 ml of a 0.050 M ammonium metavanadate aqueous solution (1.1697 g was dissolved in 200 ml distilled water). pH was adjusted to (2.5) with nitric acid. The suspension was kept stirred for one hour, then filtered under vacuum and dried at 70°C for twenty-four hours before calcination at 300°C for one hour (Tapia *et al.*, 2005).

2.2.3. Preparation of V_2O_5/ γ-Al_2O_3 catalyst.

V_2O_5/γ-Al_2O_3 catalyst was prepared by the impregnation method. 1.00 g of γ-Al_2O_3 and 0.229 g of ammonium metavanadate dispersed in 19.5 ml distilled water in 250 ml beaker while stirring and kept for twenty-four hours. Then placed in a drying oven at 100°C overnight before calcination at 600°C for two hours under O_2 atmosphere (He *et al.*, 2009).

2.2.4. Preparation of V-Ni-O catalyst.

3.4025 g of nickel acetate powder was added to a basic hot aqueous solution containing 1.1478 g of ammonium metavanadate was dissolved in 120 ml distilled water in a 250 ml beaker. The pH was adjusted to pH=9 by adding aqueous ammonia. The mixture was stirred for one hour. The resulting suspension was evaporated to dryness at 85°C, and then followed by further drying at 95°C for twelve hours. The dried powder was crushed and calcined under an oxygen atmosphere at 600°C for four hours (Mattos *et al.*, 2002).

2.2.5. Preparation of V-Ni-Mg-O catalyst.

0.4290 g of magnesium hydroxide powder and 1.7012 g of nickel acetate were added to a basic hot aqueous solution containing 1.1478 g of ammonium metavanadate was dissolved in 120 ml distilled water in a 250 ml beaker. The pH was adjusted to pH=9 by adding aqueous ammonia the mixture was stirred for one hour. The resulting suspension was evaporated to dryness at 85°C and then followed by further drying at 95°C for twelve hours. The dried powder was crushed and calcined under an oxygen atmosphere at 600°C for four hours (Mattos *et al.*, 2002).

2.2.6. Preparation of V_2O_5- Mg-O/ γ-Al_2O_3 catalyst.

V_2O_5-Mg-O/γ-Al_2O_3 catalyst was prepared by the impregnation method. 1.00 g of γ-Al_2O_3, 1.7161 g of magnesium hydroxide, and 1.1478 g of ammonium metavanadate dispersed in 22 ml distilled water in 250 ml beaker while being stirred and kept for 24 hours. Then placed in a drying oven at 100°C overnight before calcination at 600°C for two hours under O_2 atmosphere (He *et al.*, 2009).

2.2.7. Preparation of V_2O_5- Ni-O/ γ-Al_2O_3 catalyst.

V_2O_5- Ni-O/ γ-Al_2O_3 catalyst was prepared by the impregnation method. 1.00 g of γ-Al_2O_3, 6.8049 g of nickel acetate, and 1.1478 g of ammonium metavanadate dispersed in 25 ml distilled water in 250 ml beaker while stirring and kept for twenty-four hours. Then placed in a drying oven at 100°C overnight before calcination at 600°C for two hours under O_2 atmosphere (He *et al.*, 2009).

2.2.8. Preparation of V_2O_5- Ni- Mg-O/ γ-Al_2O_3 catalyst.

V_2O_5- Ni-Mg-O/ γ-Al_2O_3 catalyst was prepared by the impregnation method. 1.00 g of γ-Al_2O_3, 6.8049 g of nickel acetate, 0.8580 g of magnesium hydroxide, and 1.1478 g of ammonium metavanadate dispersed in 25 ml distilled water, while being stirring and kept for 24 hours. Then placed in a drying oven at 100°C overnight before calcination at 600°C for two hours under O_2 atmosphere (He *et al.*, 2009).

2.2.9. Calcination

Calcination is a thermal treatment carried out in an oxidizing atmosphere (O_2 atmosphere) at temperatures above the projected operating temperature of the catalyst. The purpose of the calcination is to stabilize the physical and chemical properties of the catalyst and to remove any unwanted substances at the catalyst surface (impurities). Samples weighing ~0.500 g of each catalyst were placed on the catalyst bed in the reactor, then treated with O_2 gas at high temperature (see Tables 1 and 2) for a certain time period (1-4 hours), as shown in Fig. 1.

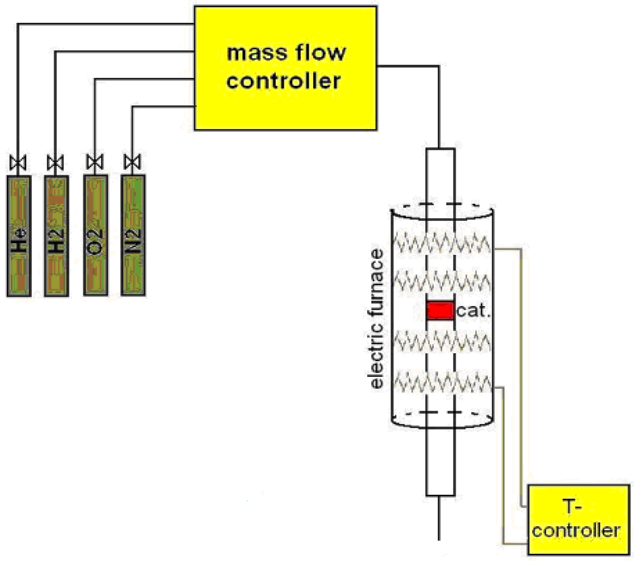

Fig.1. Experimental set-up of thermal treatment and calcination apparatus.

2.2.10. Sample preparation for AAS analysis

For each one of the prepared catalysts, the following procedure was applied: 0.2000 g of the prepared catalyst was dissolved in approximately 20 ml of concentration. nitric acid added to 60 ml of concentration. hydrochloric acid (Aqua-Regia) in a 250ml beaker. The solution was heated to boiling over a hot plate when all catalyst materials were dissolved (except the catalysts support γ-Al_2O_3), the volume of the solution was reduced to about 10 ml by evaporation. The solution was then allowed to cool before being transferred to a 100 ml volumetric flask and diluted with distilled water to the mark. Exactly 2.00 ml of the previous solution were then diluted to 100 ml in another 100 ml volumetric flask.

2.3. Catalyst characterization

2.3.1. X-ray diffraction (XRD)

The prepared catalysts were characterized by means of x-ray powder diffraction (XRD) aiming at identifying the crystalline

phases in the prepared catalysts. XRD measurements were performed for the ready to use a catalyst in the department of archeology at Yarmouk University using Shimadzu LabX device with a Fe-K_α-tube (λ=1.93 Å) in the range of 2θ=10-100º and a scanning rate of 1°/min.

2.3.2. Transmission Electron Microscopy (TEM)

Selected catalysts were characterized by using transmission electron microscopy (TEM). TEM was used to evaluate the size and shape of the metallic phase on the catalyst surface. The metallic phase is optically more opaque than the support and appears as dark spots in the micrographs. All micrographs have been taken with an electron energy of 80 kev.

2.3.3 FT-IR-spectroscopy

The prepared catalysts were characterized with respect to their chemical structure by means of infrared spectroscopy. The IR-spectrum of each catalyst was measured after it had been dried overnight at 120°C. Thin wafers of the catalyst sample were prepared by mixing with KBr (Pike Technologies, Spectroscopic Grade) and the measurements were carried out using a Bruker-FTIR Tensor 27 spectrometer.

2.3.4 H^1-NMR Spectrometry

Samples of the reaction mixtures were analyzed in the Chemistry Department at Yarmouk University using (Bruker Avance III 400MHz). This was done after bubbling the exiting gaseous reaction mixture in $CDCl_3$ solvent.

2.4. Oxidation reactions

2.4.1. Experimental set-up

Fig. 2 is a schematic representation of the experimental set-up to carry out both, the oxidative dehydrogenation and total oxidation reactions. These reactions were carried out in a Pyrex fixed-bed flow reactor (46 cm long X 2.2 cm wide) with a fritted disc placed 10 cm above the bottom heated by means of a tubular programmable electric furnace (GSL1100X, MTI Corporation). Gases flow rates were controlled by a four-channel electronic mass flow controller (Matheson-8274), sample analysis was performed by gas chromatography (G.C) as follows: the reaction mixture was analyzed by gas chromatography (HP 5890) with a thermal conductivity detector connected to a peak simple.

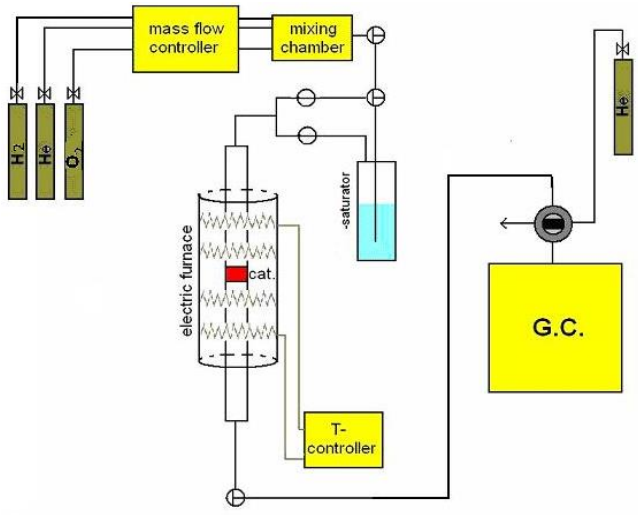

Fig. 2. Experimental set-up of the oxidation of propane.

Chromatography integration system (SRI 203) consists of the injector, detector, and column temperatures of 100, 150, and 55°C, respectively. The used column was a 23% SP-1700, 80% Chromosorb paw, packed s.s 1/8"x 30'.

2.4.2. Reactions

Samples weighing ~0.200 g of the different catalysts were placed on the catalyst bed of the reactor (Fig. 2). Helium gas was followed by oxygen gas and then passed over the catalyst in the reactor (downward) while heating from room temperature to 500°C (10°C/min). After that, the catalyst is kept under these conditions for one hour to ensure surface cleaning (oxidation of all impurities), the calcination process is performed using the device shown in (Fig. 2) through its programming and by raising the temperature from the room temperature which represents (C_1) in the device to the required degree 500 which represents (C_2) and the time required is calculated to make the conversion process, which represents (T_1) by the following calculation[(C_2-C_1)/(10°C/min)]. Then programmed to stay on this required degree, which is 500°C and 600°C for some catalysts, which represents (C_3) by determining the time that the sample should remain at this degree, which is represented by T_2. The system was then cooled down to 300°C where propane gas was introduced at different flow rates (with different O_2/propane ratios). After that, the reactor temperature was increased gradually up to 500°C and 600°C for some catalysts (3°C/min). While analyzing the reaction mixture approximately every 20°C increment, this is to study the temperature effect on both, the catalyst activity and selectivity. To investigate the effect of changing the O_2/propane ratio, the flow rates of the used gases were changed as follows, (Table 1).

Table 1

Flow rate (ml/min) of He, O_2, and propane gases used in the oxidation reactions.

He gas flow rate (ml/min)	O_2 gas flow rate (ml/min)	Propane gas flow rate (ml/min)
60	21	21
60	34	17
60	10	30
60	9	36

3. Results and Discussion

3.1. X-ray Diffraction

X-ray diffraction has been applied to identify the crystalline phases of the various catalytic systems investigated in this work (Sajid, 2015). It is known that NiO and MgO which exhibit similar diffraction patterns. This is because Ni^{2+} and Mg^{2+} ions have similar valencies, ionic radii [r(Ni^{2+}) = 0.07 nm and r(Mg^{2+}) = 0.065 nm] and crystal cell dimensions (Ndhlovu, 2011). The following figures show the x-ray diffraction pattern for V-Ni-Mg-O and V-Ni-O catalysts in the range 2θ=42-90º. Note that the reference diffraction patterns reported in the literature are usually given for Cu tubes as a source of X-ray. Since in this work the diffraction patterns were collected using a Fe tube as an X-ray source, it is necessary to calculate the positions of the diffraction lines for the Fe tube from those for the Cu tube reported in the literature. Fig. 3 clearly shows that, as expected, the diffraction stick pattern of the reference NiO material (JCPDS 00-004-0835) is very similar to that of MgO (JCPDS 00-004-0829).

The diffraction lines of reference NiO and MgO do not match with the experimentally observed major diffraction lines of the systems V-Ni-Mg-O and V-Ni-O. Due to the compound configuration between vanadium and added oxides (NiO and MgO) the diffraction lines of reference NiO and MgO do not match with the experimentally observed major diffraction lines of the systems V-Ni-Mg-O and V-Ni-O. The thorough comparison however shows that small amounts of NiO and/or MgO are indeed present. Their corresponding diffraction features appear as small shoulders at 47°, 55° and 83°.

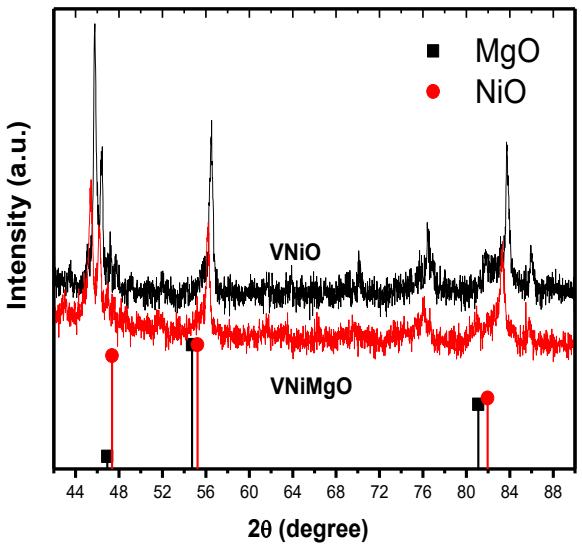

Fig. 3. X-ray diffraction patterns of V-Ni-O and V-Ni-Mg-O catalysts.

In an attempt to identify the crystalline phases of the above systems, the experimentally observed diffraction patterns were also compared with the following reference materials: V_2O_5 (00-045-1054), V_2O_5 (JCPDS 00-041-1426), V_2O_3 (JCPDS 00-039-0774), VO_2(JCPDS 00-009-0142), V_2O_3(JCPDS 00-034-0187). However, a good match was only found with the diffraction lines of $Mg_3V_2O_8$ (JCPDS 00-037-0351) and $Ni_3V_2O_8$ (JCPDS 00-037-0353) as can be seen in (Fig. 4). It is important to notice that the 2θ-scale in (Fig. 4) has been restricted to 65° because the reference cards contained no lines above this value. The experimentally observed diffraction lines in the range 2θ=65-100° (see Fig. 3) are however believed to still belong to the orthovanadate phase because it is impossible to have a phase with diffraction lines only in this high 2θ range. (The obtained diffraction patterns are compared experimentally with that found in the reference of the Mg and Ni vanadate to prove the existence of these phases in the prepared systems, but the lines of the data of diffraction stick pattern that were taken from literature of Mg and Ni vanadate do not have data beyond the angle 65 ° while it found bands at approximately (80-88) which may be attributed to orthovanadate phase).

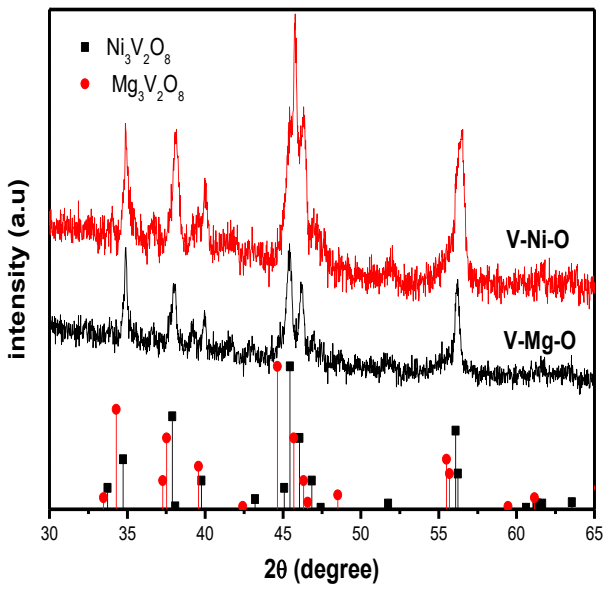

Fig. 4. X-ray diffraction patterns of V-Ni-O and V-Ni-Mg-O catalysts.

From Figs 3 and 4, the most important change in the XRD pattern that could be observed upon the incorporation of Mg in the system is that the diffraction lines become smaller indicating a lower degree of crystallinity in the Mg containing system. Fig. 5 compares the diffraction patterns of V-Ni-O and V-Ni-O-alumina. All diffraction lines of V-Ni-O, attributed to the $Ni_3V_2O_8$ phase are present in the diffraction pattern of V-Ni-O-alumina confirming thus the presence of the orthovanadate phase also in the V-Ni-alumina. However, additional sharp diffraction lines are observed in the V-Ni-O-alumina system at 47°, 55°, 57° and 83°. But V-Ni-O shows weak diffraction features at 47°, 55° and 83° (attributed above to the presence of NiO). It is therefore believed that the sharp diffraction lines at these positions in the V-Ni-O-alumina system are just better development of the corresponding weak features of V-Ni-O probably due to better crystallization. The small diffraction lines at 57° and 88° are attributed to the presence of γ-Al_2O_3.

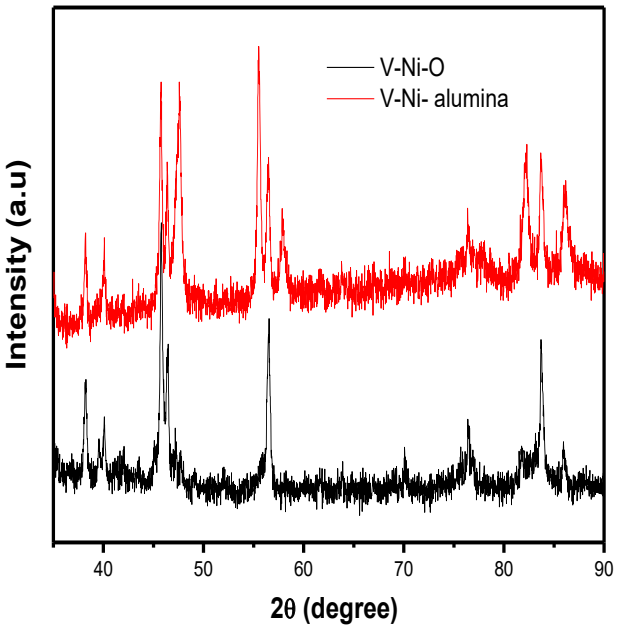

Fig. 5. X-ray diffraction patterns of V-Ni-O and V-Ni-alumina catalysts.

Fig. 6 shows the diffraction patterns of the V-Ni-O/γ-Al_2O_3, V-Ni-Mg-O/γ-$Al_2O_3$and V-Mg-O/γ-Al_2O_3 systems. The first two diffraction patterns are very similar to each other. As discussed in (Fig. 5), all diffraction lines coincide with those of the orthovanadate phase in the V-Ni-O/γ-Al_2O_3, V-Ni-Mg-O/γ-Al_2O_3 catalysts. It is interesting to notice that in the V-Mg-O/γ-Al_2O_3 system, only the diffraction lines of MgO at 55° and 83° are observed with no indication for the formation of crystalline Mg orthovanadate phase. This explains why the incorporation of Mg in the V-Ni-O system led to decreased intensities of the diffraction lines of the orthovanadate system. It is interesting to notice that each system contains two small diffraction lines at 57° and 88° which are attributed to the presence of γ-Al_2O_3.

Fig. 7 shows the diffraction patterns of the V-Ni-O/γ-Al_2O_3, V_2O_5/γ-Al_2O_3, and VO_x/γ-Al_2O_3 systems. The patterns of V_2O_5/γ-Al_2O_3 and VO_x/γ-Al_2O_3 systems are very similar to each other but these compounds V_2O_5, VO_2, or V_2O_3 could not be determined. The difference between these two patterns and that of V-Ni-O/γ-Al_2O_3 is attributed to the absence of the vanadate phase in the V_2O_5/γ-Al_2O_3 and VO_x/γ-Al_2O_3 systems. But the diffraction line at 57° and 88° in the V_2O_5/γ-Al_2O_3 and VO_x/γ-Al_2O_3 systems is similar to that observed in V-Ni-O/γ-Al_2O_3 and is attributed to the presence of γ-Al_2O_3 as previously mentioned.

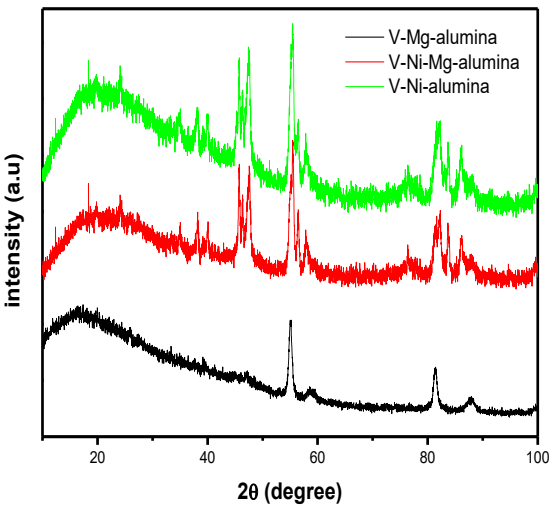

Fig. 6. X-ray diffraction patterns of the V-Ni-O/γ-Al_2O_3, V-Ni-Mg-O/γ-Al_2O_3, and V-Mg-O/γ-Al_2O_3 systems.

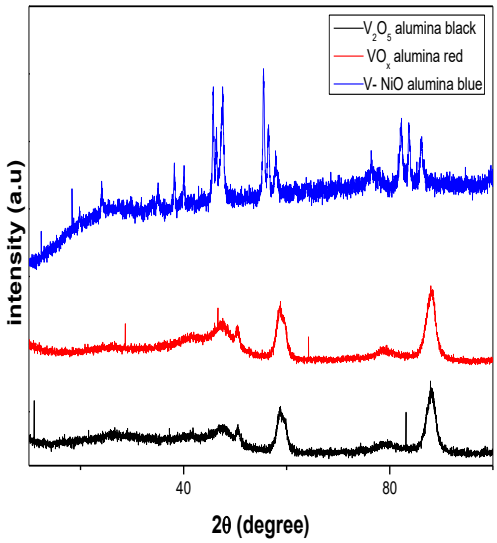

Fig .7. X-ray diffraction patterns of the V-Ni-O/γAl_2O_3, V_2O_5/γ-Al_2O_3 and VO_x/γ-Al_2O_3 systems.

3.2. Transmission Electron Microscopy (TEM)

TEM among other applications is used for determining the size and shape of metal nanoparticles. The application of this technique is based on the fact that the electron transmittance of the oxide support is larger than that of the supported metal and the support would thus appear in the micrograph brighter than the metal. Dark patches corresponding to the oxide support may be also appeared due to the aggregation of the oxide phases over each other leading to the depressed transmission of electrons (Challa, 2014).

Fig. 8 represents a TEM-micrograph of V-Ni-Mg-Oxide catalyst. The observed particle size of V-Ni-Mg oxides is about 46-192 nm. The particles which vary in shape, ranging from spherical to oval and orthorhombic (Samir, 2019; Nor, 2011) which is clearly appeared in Fig. 8.

On the other hand, the V_2O_5- Ni-O/ γ-Al_2O_3 catalyst appears to form the cubic particles, in addition to the previous forms. Fig. 9 shows the particles' shapes, and size of this catalyst ranging from 14-196 nm. Fig. 10 shows the particle size for catalyst V-Ni-O ranging from 16-195 nm, and with mixed particles shapes.

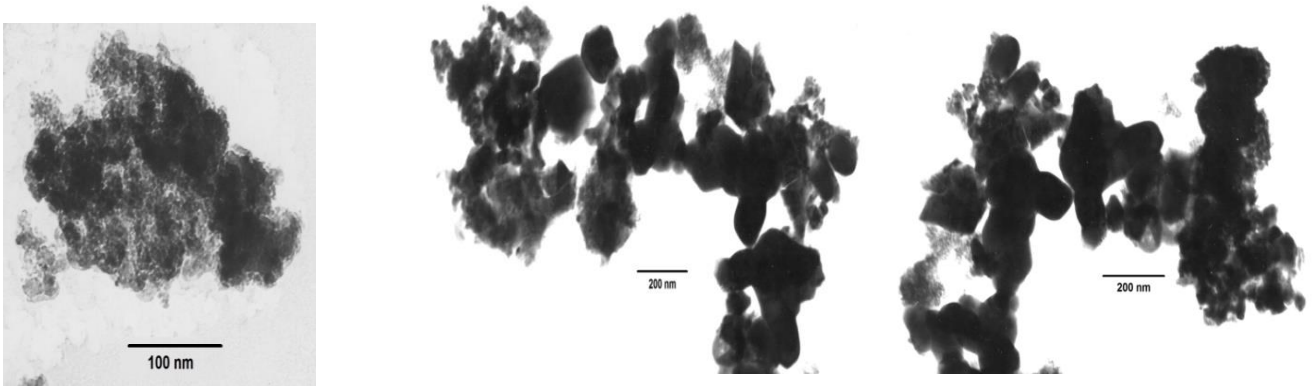

Fig. 8. TEM-micrographs of V-Ni-Mg -O at 80 kev.

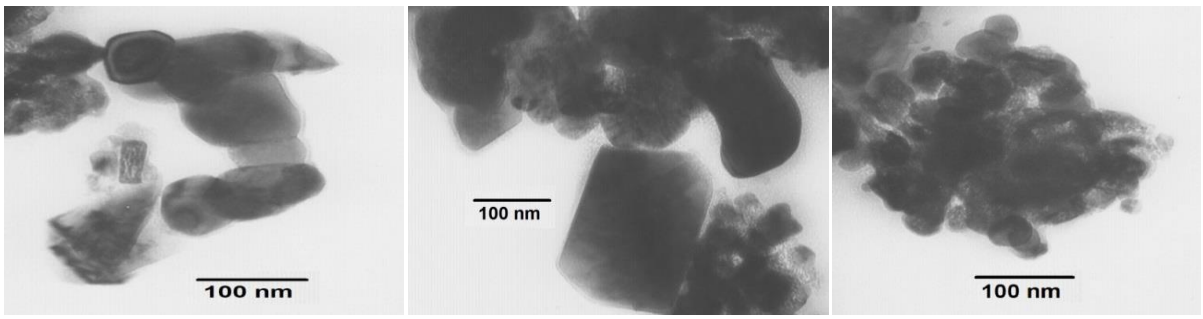

Fig. 9. TEM-micrographs of V_2O_5- Ni-O/ γ-Al_2O_3 at 80 kev.

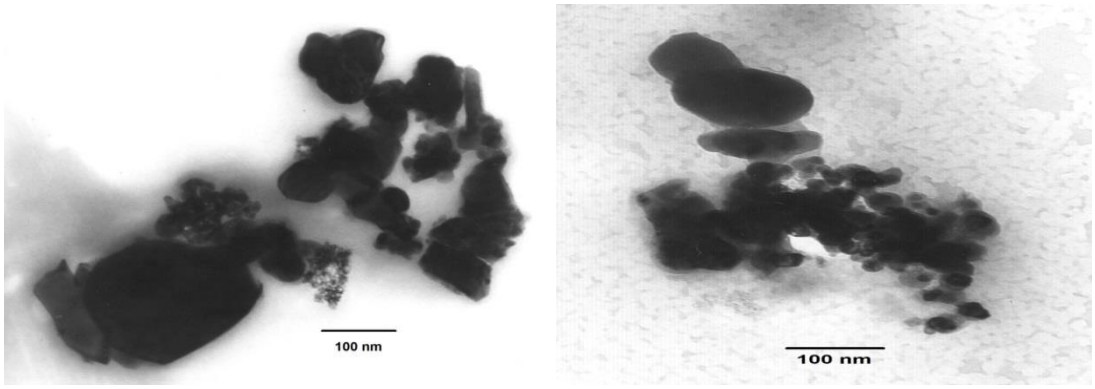

Fig . 10. TEM-micrographs of V- Ni-O at 80 kev.

3.3. Atomic Absorption Spectrophotometry (AAS)

Table 2 shows the results of AAS analysis of the prepared catalysts where the results are expressed in mg/L (ppm) unit. Moreover, the molar ratios of the three metal components were calculated and listed in (Table 3).

Table 2

AAS results in mg/L (ppm) unit for the prepared catalysts.

Catalyst (theoretical composition)	[Ni] (mg/L)	[Mg] (mg/L)	[V] (mg/L)
Mg_3-V_2-O_8	0	40.5	30.1
Ni_3-V_2-O_8	89.4695	0	52.3
V_1-Ni_3-O/γ-Al_2O_3	463	0	118
V_1-Mg_3-O/γ-Al_2O_3	0	58.062	37.8
V_2-$Ni_{1.5}$-$Mg_{1.5}$-O_8	174	81.3	131
V_1-$Ni_{1.5}$-$Mg_{1.5}$-O/ γ- Al_2O_3	57.0225	28.988	37.2

Table 3

Molar ratios of prepared catalysts components.

Catalyst (theoretical composition)	Ni	Mg	V
Mg_3-V_2-O_8	0	2.8	1
Ni_3-V_2-O_8	3	0	2
V_1-Ni_3-O/γ-Al_2O_3	3	0	1
V_1-Mg_3-O/γ-Al_2O_3	0	3	1
V_2-$Ni_{1.5}$-$Mg_{1.5}$-O_8	2.3	2.6	2
V_1-$Ni_{1.5}$-$Mg_{1.5}$-O/ γ- Al_2O_3	1.3	1.6	1

The calculated ratios for Ni:Mg:V are acceptable and very close to the anticipated values. For example Ni_3-V_2-O it was calculated as follows (weight of V (1.15 g)*mass number of V)/molecular mass of starting material of ammonium metavanadate, the obtained value represents the weight of the vanadium in the ammonium metavanadate) in the same way, the weight of the nickel is calculated with the difference in molecular mass, so that it is the starting material nickel acetate. The obtained weights are then divided by the mass number of each metal then converted to integers.

3.4. IR spectroscopy

3.4.1 IR spectroscopy of V_2O_5/ γ-Al_2O_3 catalyst.

Fig. 11 shows the IR spectra of calcined V_2O_5/γ-Al_2O_3 catalyst, before and after the catalytic reaction, and of VO_x/ γ-Al_2O_3 after the reaction. All three spectra are characterized by broad strong absorption in the range 400-1000 cm^{-1} corresponds to Al-O vibration (Hosseini *et al.*, 2011). This conclusion is supported by the fact that a small band is observed at ~1397 cm^{-1} which could be assigned to the longitudinal acoustic mode of vibration of alumina (Tapia *et al.*, 2004).

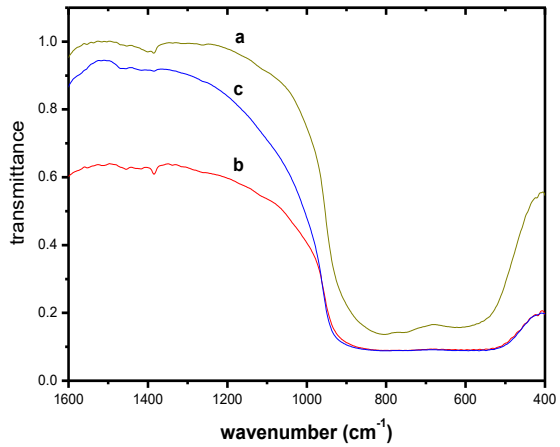

Fig.11. IR spectra of calcined V_2O_5/ γ-Al_2O_3 catalyst a) before and b) after the reaction, and of c) VO_x/ γ-Al_2O_3 catalyst after the reaction.

The two spectra of V_2O_5/γ-Al_2O_3 before and after the reaction (**a** and **b** in Fig. 11) are very similar to each other, indicating that the reaction did not change the vibrational properties of the system. In addition, the IR spectrum of VO_x/ γ-Al_2O_3 after the reaction is very similar to the other two spectra indicating that the two systems are very similar. The absence of V_2O_5 can be inferred from the absence of V=O characteristic band at ~1020 cm^{-1} vibration mode (Mattos *et al.*, 2002).

3.4.2. IR spectrum of V_2O_5-Mg/ γ-Al_2O_3 catalyst.

Fig. 12 shows the IR spectra of V_2O_5-Mg/γ-Al_2O_3 before and after the reaction. The differences between the two spectra are considered below:

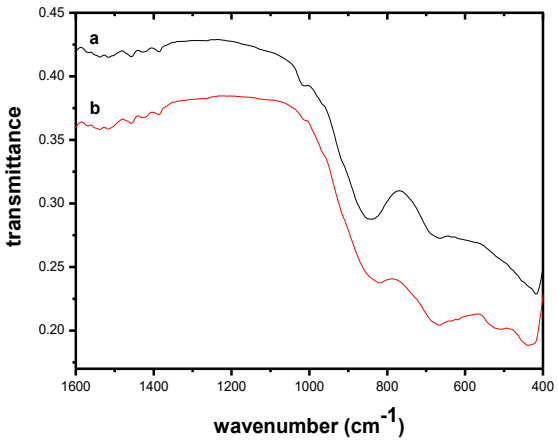

Fig.12. IR spectrum of V_2O_5-Mg/ γ-Al_2O_3 catalyst a) before and b) after the reaction.

Before reaction, a rather tiny absorption feature is observed around 1019 cm^{-1} which is characteristic for the V=O vibration in V_2O_5 (Mattos *et al.*, 2002). This suggests the presence of V_2O_5, after the reaction, this band becomes very small indicating that the V=O group has been reacted off during the reaction. The IR spectrum of V_2O_5-Mg/γ-Al_2O_3 before reaction shows a shoulder at 920 cm^{-1} and two bands at 847 cm^{-1} and 675 cm^{-1}, all of which can be attributed to the vibrations of Mg orthovanadate phase (Mattos *et al.*, 2002). After the reaction, there is no significant change of these bands, but two new absorption features become pronounced at 525cm^{-1} and 825cm^{-1}. This can be attributed to the stretching vibration of V-O-V group belonging to the V_2O_5 phase (Brown and Stewart, 1970).

3.4.3. IR spectrum of V-Mg-O and V-Ni-O catalysts.

Fig. 13 shows the IR spectra of V-Ni-O and V-Mg-O catalysts, which are very similar. It can be clearly seen that all absorption bands of V-Ni-O are with a small shift to higher frequencies of those of V-Mg-O. However, all these bands are at 920 cm^{-1}, 847$cm^{-1}$and 675cm^{-1}, all of which can be attributed to the vibrations of Mg orthovanadate and Ni orthovanadate phases (Tapia *et al.*, 2004; Mattos *et al.*, 2002), that agree with the results of XRD. The bands in the case of V-Ni-O are much more pronounced than those in the case of V-Mg-O probably due to the better order in the V-Ni-O system as indicated by XRD measurements (Fig. 4 and Fig. 5).

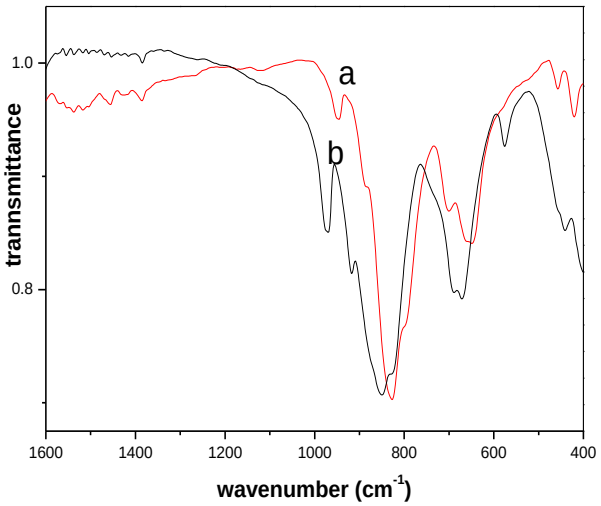

Fig .13. IR spectrum of calcined a) V-Mg-O and b) V-Ni-O catalysts.

3.4.4. IR spectrum of V-Mg-O, V_2O_5-Mg-O/γ-Al_2O_3 catalysts, and of pure γ-Al_2O_3.

Fig. 14 compares the absorption properties of V-Mg-O and V_2O_5-Mg-O/γ-Al_2O_3. The absorption bands that appear at 847cm^{-1} and 675 cm^{-1}can be attributed to the vibrations of Mg orthovanadate phase which is present in both systems (V-Mg-O and V_2O_5-Mg-O/γ-Al_2O_3). But V_2O_5-Mg-O/γ-Al_2O_3 shows weaker absorption bands when compared to V-Mg-O. Moreover, V_2O_5-Mg-O/γ-Al_2O_3 contains a tiny absorption band at 1019 cm^{-1} which is characteristic of the V=O vibration in V_2O_5 (Mattos et al., 2002). This band is not present in V-Mg-O. IR spectroscopy indicates the formation of V_2O_5 that contains V=O bonds in the V_2O_5-Mg-O/γ-Al_2O_3 catalyst. Fig. 14 shows also the IR spectra of pure γ-Al_2O_3 with two broad band's at around 604 cm^{-1} and 805 cm^{-1} which can be attributed to Al-O vibrational mode, and a small band observed at ~1397 cm^{-1} which could be assigned to the longitudinal acoustic mode of vibration of alumina (Ma *et al.*, 2008).

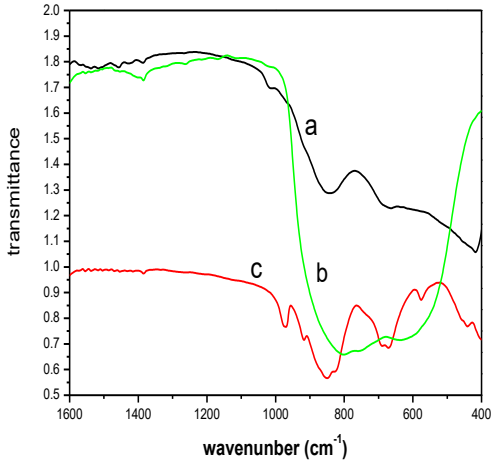

Fig.14. IR spectrum of a) V-Mg-O/γ-Al_2O_3, b) pure γ −alumina and c) V-Mg-O catalysts.

3.5 ^{1}H-NMR identification of the catalytic reaction products.

The detection and composition structures of the reaction products were confirmed by ^{1}H-NMR (BRUKER AVANCE III 400 MHz) which shows (Fig. 15) the presence of CH_3 group of propene at 1.9 ppm as a doublet, CH_2 group of propene at 4.5 ppm, and at 4.6 ppm as a doublet of doublets, and the presence of CH group at 5.2 ppm as a multiplet. All these results indicate the occurrence of oxidative dehydrogenation of propane. This was done after bubbling the exiting gaseous reaction mixture in $CDCl_3$ solvent.

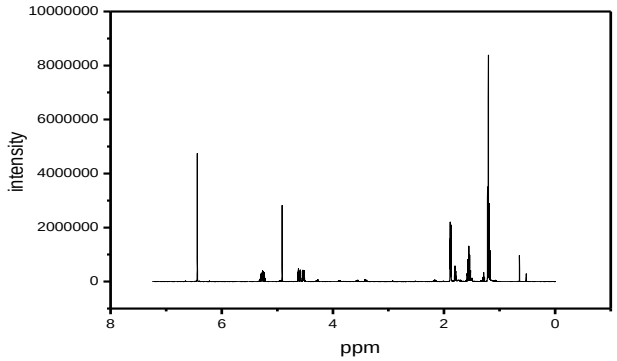

Fig. 15. ^{1}H-NMR spectrum of the reaction mixture over V-Ni-O catalyst.

Fig. 15 shows the ^{1}HNMR spectrum of the reaction mixture over V-Ni-O catalyst just as an example. This spectrum can be broken down and displayed more clearly in Fig. 16, as follows:

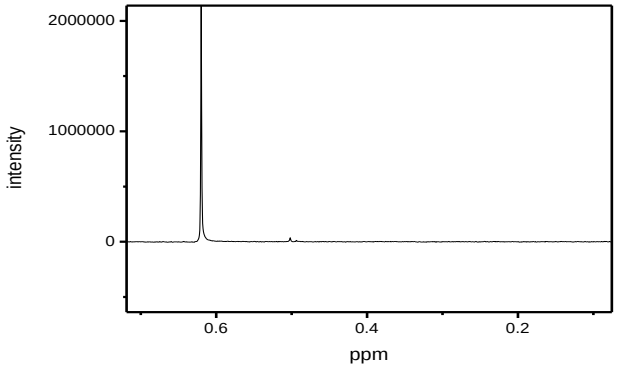

Fig . 16. ^{1}H-NMR Spectrum of methane as a singlet.

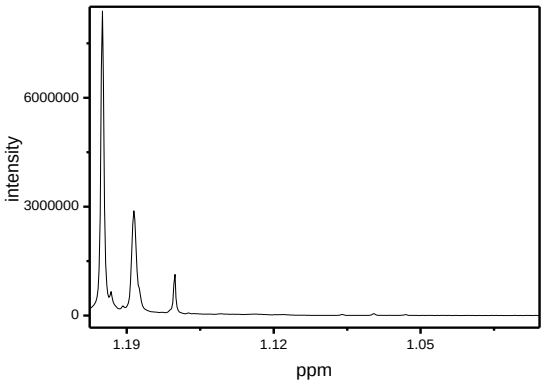

Fig . 17. ^{1}H-NMR spectrum of propane as (triplet of triplets)

Fig. 16 and Fig 17. show ^{1}H NMR spectra of methane and propane samples. The singlet signal (in Fig. 16) situated at 0.62 ppm is assigned to protons in methane, which indicates an occurrence (hydrogenolysis of propane), while the triplet of triplets peak (in Fig. 17) which observed in the range (1.17-1.20 ppm) is assigned to propane.

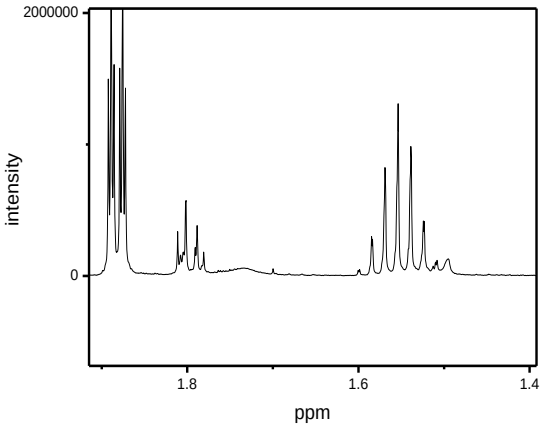

Fig. 18. ^{1}H-NMR spectrum of propane and propene

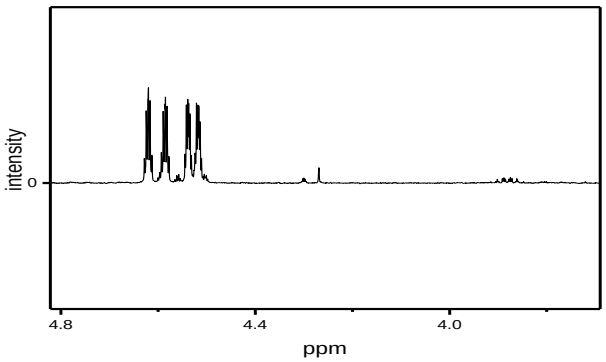

Fig. 19. ^{1}H-NMR spectrum of propene as a doublet of doublets as multiplets and doublets, respectively.

Fig. 18 and Fig. 19 show ^{1}H NMR spectra of propane and propene samples. The multiplet signals (in Fig. 18) located in the range (1.5–1.6 ppm) are assigned to protons in propane, and the doublets peak (in Fig. 18) observed at 1.9 ppm is assigned to propene, while Fig. 19 shows ^{1}H-NMR spectrum of propene as a doublet of doublets which observed at 4.5 ppm.

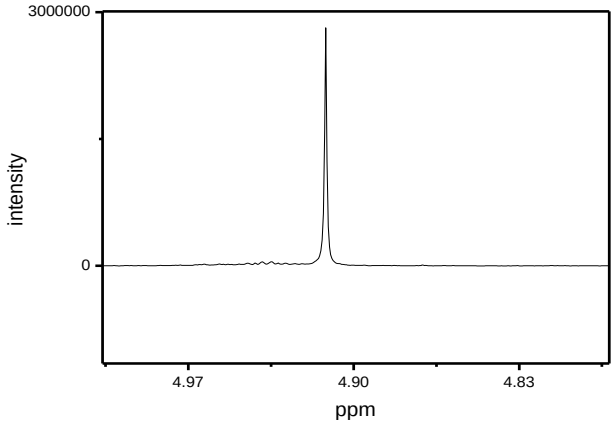

Fig. 20. ^{1}H-NMR spectrum of ethylene as a singlet.

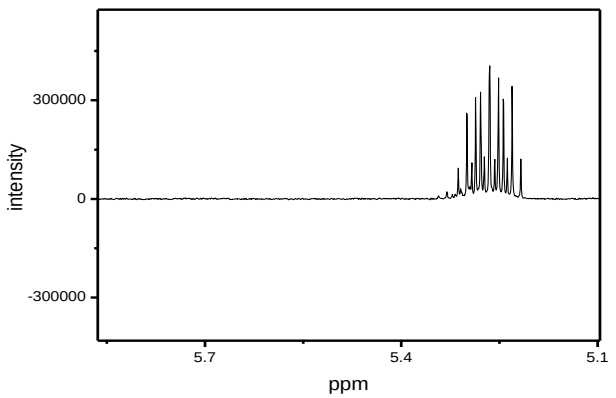

Fig. 21. ^{1}H-NMR spectrum of propene as a multiplet.

Fig. 20 and Fig. 21 show ^{1}H NMR spectra of ethylene and propene samples (oxidative dehydrogenation of propane). The singlet signal (in Fig. 20) situated at 4.92 ppm is assigned to protons in ethylene, while multiplet peaks (in Fig. 21) observed at 5.25 ppm is assigned to propene.

3.6. Gas Chromatographic analysis data of the oxidation of propane over the vanadium catalysts.

Table 4 shows the gas chromatographic analysis data for the oxidation of propane over the vanadium catalysts. The most active catalysts in the conversion of propane were V_2O_5-Ni-O/ γ- Al_2O_3 (97.5%), V_2O_5-Ni- Mg-O/ γ- Al_2O_3 (78.6%), V_2O_5- Mg-O/ γ- Al_2O_3 (78.3%), V-Ni- Mg-O (76.4%), V-Mg-O (79.31%%), and V-Ni-O (48%). At temperature (600 °C) and differ flow rate (1:1, 2:1 (O_2: propane).

Table 4

Oxidation of propane over the vanadium catalysts at reaction temperature 500°C, 600°C and calcination temperature at 600°C exceptions VO_x/ γ- Al_2O_3 was calcined at 500°C.

Catalysts Reaction temperature	V-Ni-O 600°C	V-Ni-Mg-O 600°C	V_2O_5-Ni-O/ γ-Al_2O_3 500°C	V_2O_5-Ni- Mg-O/ γ-Al_2O_3 500°C	V-Mg-O 600°C	V_2O_5/ γ- Al_2O_3 500°C	VO_x/ γ- Al_2O_3 500°C	V_2O_5 -Mg-O/ γ-Al_2O_3 600°C
% Conversion of propane	48%	76.40%	97.5%	78.6%	79.31%	13%	13%	78.3%
% Conversion (total)	0%	1.9%	76.09%	11.4%	3.06%	3%	2%	3.02%
% Conversion of propene	15%	26.6%	3.94%	24.82%	26.6%	10%	11%	23.56%

When comparing the results presented in Table 4 it can be clearly seen that the most selective catalysts in oxidative dehydrogenation of propane to propene are V-Mg-O (conv. 26.6%), V-Ni-Mg-O (conv. 26.5%) at 600°C, and V_2O_5-Ni- Mg-O/ γ-Al_2O_3(conv. 24.8%) at 500°C where the latter catalyst is considered the best because it gives the same conversion but at a lower temperature. The reason for this is probably due to the nature of these catalysts where (MgO and NiO), basic oxides are selective towards alkenes production propene (Murgia *et al*., 2004). This is because these catalysts contain VO_4 tetrahedral units (orthovanadate) which are known to be active for the oxidative dehydrogenation reactions (Mattos *et al*., 2002). Since propane molecule which is activated and adsorbed on the reactive surface oxygen of the isolated tetrahedral VO_4 units removes a hydrogen atom from the propane molecule to form an adsorbed propyl radical and a surface OH group which greatly favors the catalytic activity and selectivity to propene (Mattos *et al*., 2002). This is why the incorporation of magnesium into vanadium is a very important step because it will improve the oxidative dehydrogenation selectivity (Elkhalifa *et al*., 2018). Table 5 shows the selectivity of all vanadium catalysts used in the oxidation of propane. The most selective catalysts for propene production were VOX/γ-Al_2O_3 (84%), V2O5/ γ-Al_2O_3 (78%), V-Ni-Mg-O (35%), and V-Mg-O (33%) respectively.

Table 5

The selectivity of all vanadium catalysts used in the oxidation of propane.

Catalysts	V-Ni-O (%)	V-Ni-Mg-O (%)	V_2O_5-Ni-O/ γ-Al_2O_3 (%)	V_2O_5-Ni- Mg-O/ γ- Al_2O_3 (%)	V-Mg-O (%)	V_2O_5/ γ-Al_2O_3 (%)	VO_x/ γ-Al_2O_3 (%)	V_2O_5 -Mg-O/ γ-Al_2O_3 (%)
Selectivity to propene	30.39	34.72	4	31.56	33.47	77.92	84.075	30.06
Selectivity to total oxidation	0	2.48	78	14.54	3.85	22.07	15.92	3.86
Selectivity to ethylene	27.5	57.35	0	47.8	61.5	0	0	50.73
Selectivity to methane	42.08	5.42	17.49	6	1.15	0	0	15.34

4. Conclusion

The oxidative dehydrogenation of propane over vanadium catalysts has been studied. A series of vanadium catalysts were prepared by the adsorption equilibrium method and impregnation method. All prepared catalysts were characterized through the XRD, IR spectroscopy, and TEM techniques. The diffraction patterns in the cases of the V-Mg-O, V-Ni-Mg-O, V-Ni-O, V_2O_5-Ni-O/γ-Al_2O_3 are attributed to the presence orthovanadate phase. However, the diffraction lines become smaller with the incorporation of Mg in these systems. Moreover, the diffraction patterns of all γ-Al_2O_3 containing catalysts, show small diffraction lines at 57° and 88°, which are attributed to the presence of γ-Al_2O_3. The results of IR characterization of V-Mg-O and V-Ni-O agree with the results of XRD indicating the presence of the orthovanadate phase. TEM study showed the particle size of V-Ni-Mg-O was around 46-192 nm. In the V_2O_5-Ni-O/ γ- Al_2O_3 catalyst the particle size was in the range 14-196 nm, and 16-195 nm in the V-Ni-O catalyst. Structures of the reaction products were confirmed by ^{1}H-NMR which shows clearly the presence propene (oxidative dehydrogenation) for all catalysts. In additional, ethylene production through using V-Mg-O, V-Ni-O, V-Ni-Mg-O V_2O_5-Ni- Mg-O/ γ- Al_2O_3 and V_2O_5 -Mg-O/ γ-Al_2O_3 catalysts, and methane that indicates an occurrence (hydrogenolysis of propane) through the reaction for all catalysts, with exception to V_2O_5-Ni-O/ γ- Al_2O_3 and VO_x /γ-Al_2O_3 catalysts. All vanadium catalysts containing Mg in their composition were active in the oxidation of propane, and selective to propene (oxidative dehydrogenation). The maximum observed conversions to propene in this work were 26.6% and 24.8% were achieved by V-Mg-O, V-Ni-Mg-O, and V_2O_5- Ni-Mg-O/ γ-Al_2O_3 catalysts, respectively. The maximum observed conversion of propane by total oxidation was 76% over V_2O_5-Ni-O/ γ- Al_2O_3 catalyst prepared by the impregnation method. The main reason for the total oxidation that was observed during their reaction reverts to the strong adsorption of propene on the catalyst surface, while its desorption is difficult. In addition, the second reason depends on many factors that may affect the catalyst activity and selectivity, such as vanadium content, surface acidity, reaction temperature, feed composition (ratio of oxygen gas to propane gas). Finally, among the studied catalysts, VO_x/ γ-Al_2O_3 was most selective towards propene (84%), V-Mg-O catalyst was most selective towards ethylene production (62%), and V-Ni-O was most selective in hydrogenolysis (methane production) (42%). Moreover, V_2O_5-Ni-O/γ- Al_2O_3 catalyst was the most active catalyst (98% conv).

References

Balcaen, V., Peolman, H., Poelman, D. and Marin, G. B. (2011) 'Kinetic modeling of the total oxidation of propane over Cu- and Ce-based catalysts', *Journal of Catalysis,* 283(1), pp. 75-88.

Barsan, M. M., and Thyrion, F. C. (2003) 'Kinetic study of oxidative dehydrogenation of propane over Ni-Co molybdate catalyst', *Catalysis Today,* 81(2), pp 159-170.

Bouazza, N., Ro denas, M. A. L and Linares, S. A. (2008) 'Photocatalytic activity of TiO2-based materials for the oxidation of propene and benzene at low concentration in presence of humidity, *Applied Catalysis B: Environmental,* 84(3), pp. 691-698.

Brown, M. E., and Stewart, B. V. (1970) 'The thermal decomposition of ammonium metavanadate, I.', *Journal of thermal analysis,* 2(3), pp. 287-299.

Challa. S. S. R. Kumar. (2014) '*Transmission Electron Microscopy Characterization of Nanomaterials*', Springer: Berlin, Heidelberg. https://doi.org/10.1007/978-3-642-38934-4_3

Dimitratos, N., and Vedrine, J. C. (2003) 'Role of acid and redox properties on propane oxidative dehydrogenation over polyoxometallates', *Catalysis Today,* 81(4), pp. 561-571.

Elkhalifa, E. A., and Friedrich, H. B. (2018) 'Magnesium oxide as a catalyst for the dehydrogenation of n-octane', *Arabian Journal of Chemistry,* 11(7), pp. 1154-1159.

Haracleous, E., Machli, M., Lemonidou, A. A. and Vasalos, I. A. (2005) 'Oxidative dehydrogenation of ethane and propane over vanadia and molybdena supported catalysts', *Journal of Molecular Catalysis A: Chemical,* 232(1), pp. 29-39.

He, Y., Ji, H., Xu, J. and Wang, L. (2009) 'Deep oxidation in propane oxidative dehydrogenation to propene over V2O5/γ-Al2O3 studied by in-situ DRIFTS', *Journal of Natural Gas Chemistry*, 18(3), pp. 359-364.

Hosseini, S. A., Niaei, A. and Salari, D. (2011) *'Production of γ-Al2O3 from Kaolin', Open Journal of Physical Chemistry,* 1(2), pp. 23-27. doi: 10.4236/ojpc.2011.12004.

Livage, J. (2010) 'Hydrothermal Synthesis of Nanostructured Vanadium Oxides', *Materials*, 3, pp. 4175-4195.

Lu, Y., Wang, E., Chen, J., Qi, Y., Hu, C., Xu, L. and Peng, J. (2004) 'Hydrothermal synthesis and crystal structure of a layered vanadium oxide with an interlayer metal coordination complex: [Co(phen)3][V10O26]·H2O', *Journal of Solid State Chemistry,* 177(3), pp. 946-950.

Ma, C., Chang, Y., Ye, W., Shang, W. and Wang, C. (2008) 'Supercritical preparation of hexagonal γ-alumina nanosheets and its electrocatalytic properties', *Journal of Colloid and Interface Science,* 317(1), pp. 148-154.

Magon, C. J., Lima, J. F., Donoso, J. P., lavayen, V., Benavente, E., Navas, D. and Gonzalez, G. (2012) 'Deconvolution of the EPR spectra of vanadium oxide nanotubes', *Journal of Magnetic Resonance*, 222, pp. 26-33.

Mattos, A. M., Gil, R. S., Pocco, M. M. and Eon, J. G. (2002) 'Zinc-modified, alumina-supported vanadium oxides as catalysts for propane oxidative dehydrogenation', *Journal of Molecular Catalysis A: Chemical,* 178(1), pp. 229-237.

Mishakov, L. V., Vedyagin, A. A., Bedilo, A. F., Zaikovskii, V. I. and Klabunde, K. J. (2009) 'Aerogel VOx/MgO catalysts for oxidative dehydrogenation of propane', *Catalysis Today,* 144(3), pp. 278-284.

Murgia, V., Sham, E., Gottifredi, J. C. and Torres, E. F. (2004) 'Oxidative Dehydrogenation Of Propane And N-Butane Over Alumina Supported Vanadium Catalysts', *Latin American Applied Research*, 34, pp. 75-82.

Ndhlovu, P. (2010) Characterization of coke obtained over MgO-modified Ni/SiO2 in the decomposition of methane. MSc dissertation, University of the Witwatersrand, Johannesburg.

Nor. F.C., Nurhanna. B., Roshidah. R., Norashikin, K. and Norlida. K. (2011) *AIP Conference Proceedings,* 1400, 328. https://doi.org/10.1063/1.3663137

Pavlova, S. N., Sadykov, V. A., Frolova, Y. V., Saputina, N. F., Vedenikin, P. M., Zolotarskii, I. A. and Kuzmin, V. A. (2003) 'The effect of the catalytic layer design on oxidative dehydrogenation of propane over monoliths at short contact times', *Chemical Engineering Journal,* 91(2), pp. 227-234.

Routray, K., Reddy, K. K. and Deo, G. (2004) 'Oxidative dehydrogenation of propane on V2O5/Al2O3 and V2O5/TiO2 catalysts: understanding the effect of support by parameter estimation', *Applied Catalysis A: General,* 265(1), pp. 103-113.

Sajid, B., and Jingbo, Li. (2015) *Advanced Nanomaterials and their Applications in Renewable Energy*. 1st Edition, Amsterdam: Elsevier Science.

Samir, A. l., Hanan. F. Al., Ayman. M. M., (2019) 'An Eco-friendly Synthesis of V_2O_5 Nanoparticles and Their Catalytic Activity for the Degradation of 4-Nitrophrnol', *Journal of Inorganic and Organometallic Polymers and Materials,* 29, pp. 1324–1330. https://doi.org/10.1007/s10904-019-01096-1

Tapia, L. B., Wang, J.A., perez, I. H., rios, G. A. and Schacht, P. (2004) 'Physicochemical and textural characterization of vanadium–magnesium mixed oxides', *Materials Letters*, 58(24), pp. 3034-3039.

Tapia, L. B., Perez, I. H., Schacht, P., Cordava, I. R. and Riso, G. A. (2005) 'Influence of reducibility of vanadium–magnesium mixed oxides on the oxidative dehydrogenation of propane', *Catalysis Today,* 107-108, pp. 371-376.